Wind and Airflow Angle Estimation Using an Adaptive Extended Rauch-Tung-Striebel Smoother

Fang, X.; de Visser, C.C.; Pool, D.M.; Holzapfel, Florian

DOI
10.2514/6.2022-1399

Publication date
2022

Document Version
Final published version

Published in
AIAA SCITECH 2022 Forum

AIAA SciTech Forum
January 3-7, 2022, San Diego, CA & Virtual
AIAA SCITECH 2022 Forum

10.2514/6.2022-1399

Wind and Airflow Angle Estimation Using an Adaptive Extended Rauch-Tung-Striebel Smoother

Xiang Fang* and Florian Holzapfel†
Technical University of Munich, 85748 Garching, Germany

Coen C. de Visser‡ and Daan M. Pool§
Delft University of Technology, 2629 HS Delft, The Netherlands

This paper proposes a new method that estimates the three-dimensional stochastic wind velocity for an aircraft equipped with a Pitot-static tube and airflow vanes. Since the performance of most state estimators, e.g., the extended Rauch-Tung-Striebel smoother, relies on the process and measurement noise covariance settings, the proposed method employs the expectation-maximization approach to estimate the noise covariance matrices to improve the estimation accuracy. Numerical simulations demonstrated that the proposed method can successfully estimate the noise covariance matrices, especially for the noise covariance of the wind velocity, using the measurement data and reconstruct the wind velocity offline. Additionally, the smoothed true airspeed, angle of attack, and angle of sideslip data are more accurate compared to the direct measurements. This feature is also beneficial for other applications such as the aerodynamic model identifications of aircraft.

I. Introduction

Wind sensing and estimation from aircraft flight data is an essential topic for aerospace and atmospheric studies, such as energy harvesting [1] and wind turbulence research [2]. Furthermore, another issue associated with this topic is the estimation of airspeed and flow angles. When it comes to identifying the aircraft aerodynamic model using system identification techniques [3, 4], it is also beneficial to obtain an accurate estimation of airspeed and flow angles since the aerodynamic forces and moments have a strong dependency on these variables.

A large amount of research has been conducted on wind estimation. The main existing methods can be categorized into two types based on whether they depend on knowledge of the aircraft aerodynamic model or not, i.e., model-aided methods (e.g., [5, 6]) and model-free ones. For aircraft system identification applications, since the overall goal is to model the aircraft aerodynamics, it is necessary to consider the aerodynamic model as unknown for the wind estimation problem. Therefore, we mainly focus on the state-of-the-art for model-free methods in this paper. Langelaan et al. [1] presented a method to directly calculate the three-dimensional (3D) wind velocity by using data from the aircraft autopilot. A moving-average filter is applied post-hoc to reduce noise. Besides such direct methods, some researchers formulate wind estimation as a state estimation problem and solve it using nonlinear Kalman filters. Cho et al. [7] proposed a wind estimation method based on the Extended Kalman Filter (EKF) using measurements from a Global Positioning System (GPS) receiver and a Pitot tube. In the method proposed by Cho et al. [7] the wind velocity is assumed to be close to constant with the vertical component being zero. Also, the algorithm requires a circle flying pattern to ensure observability. To estimate the 3D wind velocity, Rhudy et al. [8] developed a solution for both the EKF and an unscented Kalman filter using inertial measurement unit (IMU), GPS, Pitot tube, and airflow vane data. Flight testing results show that this algorithm can successfully achieve satisfying estimates. In [8], the dynamics of wind velocity are modeled as a random-walk process with relatively larger process noises, compared to [7], to reflect the stochastic nature of wind rather than assume the wind velocity to be constant.

It is often more practical to model wind as a stochastic process instead of constant values considering that wind can be described as a superposition of not only mean (constant) wind, but also discrete gusts and turbulence [9] which are inherently stochastic. Rhudy et al. [10] showed that the random-walk process model is a good time-domain stochastic model for the wind and that it is easily embedded in a Kalman filtering framework. For a certain flight, the noise level in

*Doctoral Student, Institute of Flight System Dynamics, Boltzmannstraße 15. Student Member AIAA
†Professor, Institute of Flight System Dynamics, Boltzmannstraße 15. Associate Fellow AIAA.
‡Assistant Professor, Control and Simulation Section, Faculty of Aerospace Engineering, Kluyverweg 1. Member AIAA.
§Assistant Professor, Control and Simulation Section, Faculty of Aerospace Engineering, Kluyverweg 1. Senior Member AIAA.

the random walk is unknown and can vary strongly, which makes the tuning of the noise covariance in the random-walk model a non-trivial problem. Therefore, the objective of this research is to develop an adaptive smoothing algorithm to solve this noise covariance tuning problem for an optimal wind estimation.

Several studies have attempted to estimate the noise covariances in a general Kalman filtering (or smoothing) framework which can be utilized as mathematical tools for solving our problem. The Myers and Tapley (MT) approach [11] estimates the process ($\boldsymbol{Q}$) and measurement noise ($\boldsymbol{R}$) covariance matrices with a covariance matching technique using the innovation in the EKF. Based on the MT approach, de Mendonça et al. [12] proposed an adaptive filtering algorithm for online aircraft flight path reconstruction. Besides the main filter that deals with the state estimation, the authors designed two parallel Kalman filters to estimate the process and measurement noise covariances to improve the main filter's performance. For an Extended Rauch-Tung-Striebel Smoother (ERTSS)-based state estimation, Bavdekar et al. [13] proposed an extended expectation-maximization (EM) method, which is based on the maximum likelihood principle, to identify $\boldsymbol{Q}$ and $\boldsymbol{R}$. Ananthasayanam et al. [14] carried out a comparison study on different adaptive filter tuning methods for the $\boldsymbol{Q}$ and $\boldsymbol{R}$ estimation in a Kalman filtering or smoothing problem. They reported that the extended EM method is a better option for estimating $\boldsymbol{Q}$ and $\boldsymbol{R}$ than the MT approach.

Currently, these noise covariances estimation techniques have not been used in wind estimation problems. In the previous wind estimation works, such as [7, 8], the noise covariance of the random-walk wind model is set to a certain value which is chosen based on experience. Instead, in this paper, we propose to apply the extended EM method to adaptively estimate the $\boldsymbol{Q}$ and $\boldsymbol{R}$ in the wind estimation problem, especially to cope with the wind noise covariance which is different in each flight. In this work, the wind velocity is modeled as a random-walk process with the noise covariance representing the possible changing rate of the wind velocity. The random-walk model of wind velocity is integrated into the ERTSS framework as state equations. By applying the extended EM method, the noise covariance matrices $\boldsymbol{Q}$ and $\boldsymbol{R}$ can be estimated from the flight data. With the adaptively estimated $\boldsymbol{Q}$ and $\boldsymbol{R}$, the ERTSS can optimally estimate the 3D stochastic wind velocity as well as the air triplets: true airspeed V_{TAS}, angle of attack α, and angle of sideslip β in offline analyses.

This paper is organized as follows. The mathematical formulation of the wind estimation problem for this paper is introduced in Section II . To solve this problem, the proposed adaptive ERTSS method for wind estimation problem is discussed in Section III . Results based on numerical simulations are presented in Section IV to validate the proposed method. Finally, the concluding remarks are made in Section V .

II. Problem Formulation

The wind estimation problem involves solving the equations of the wind triangle. As illustrated in Fig. 1, three different velocity vectors define a vector triangle. The wind velocity vector $\boldsymbol{V}_{\mathrm{W}}$ is defined as the moving velocity of the air relative to the ground, the aerodynamic velocity vector $\boldsymbol{V}_{\mathrm{A}}$ is defined as the velocity of the aircraft relative to the surrounding air, and the kinematic velocity vector $\boldsymbol{V}_{\mathrm{K}}$ is defined as the aircraft velocity relative to the ground.

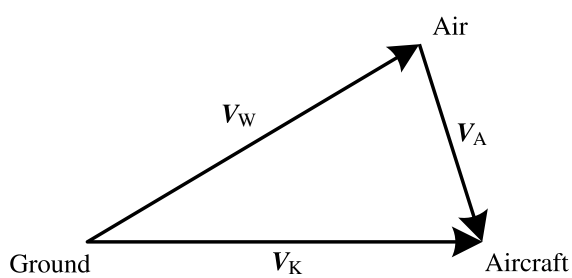

Fig. 1 The wind triangle.

Therefore, by the definition above, the wind triangle can be written as

$$\boldsymbol{V}_{\mathrm{A}} = \boldsymbol{V}_{\mathrm{K}} - \boldsymbol{V}_{\mathrm{W}} \,.$$

This vector equation can be written in a matrix form in the aircraft body-fixed frame [1] as

$$\begin{bmatrix} u_{\mathrm{A}} \\ v_{\mathrm{A}} \\ w_{\mathrm{A}} \end{bmatrix} = \begin{bmatrix} u_{\mathrm{K}} \\ v_{\mathrm{K}} \\ w_{\mathrm{K}} \end{bmatrix} - \boldsymbol{M}_{\mathrm{BE}} \begin{bmatrix} W_{\mathrm{x}} \\ W_{\mathrm{y}} \\ W_{\mathrm{z}} \end{bmatrix}, \tag{1}$$

where $(u_{\mathrm{A}},\ v_{\mathrm{A}},\ w_{\mathrm{A}})$ are the aerodynamic velocity components in the body-fixed reference frame, $(u_{\mathrm{K}},\ v_{\mathrm{K}},\ w_{\mathrm{K}})$ are the kinematic velocity components in the body-fixed frame, and $(W_{\mathrm{x}},\ W_{\mathrm{y}},\ W_{\mathrm{z}})$ are the north, east, and down components of the wind velocity vector in the earth-fixed local frame. The transformation matrix from the earth-fixed frame to the body-fixed frame $\boldsymbol{M}_{\mathrm{BE}}$ can be expressed using attitude Euler angles as

$$\boldsymbol{M}_{\mathrm{BE}} = \begin{bmatrix} \cos\psi\cos\theta & \sin\psi\cos\theta & -\sin\theta \\ \cos\psi\sin\theta\sin\phi - \sin\psi\cos\phi & \sin\psi\sin\theta\sin\phi + \cos\psi\cos\phi & \cos\theta\sin\phi \\ \cos\psi\sin\theta\cos\phi + \sin\psi\sin\phi & \sin\psi\sin\theta\cos\phi - \cos\psi\sin\phi & \cos\theta\cos\phi \end{bmatrix},$$

where ϕ is the bank angle, θ is the pitch angle, and ψ is the azimuth angle.

The mapping relationship from the aerodynamic velocity to the air triplets $(V_{\mathrm{TAS}},\ \alpha,\ \beta)$ is described by the following equations:

$$V_{\mathrm{TAS}} = \sqrt{u_{\mathrm{A}}^2 + v_{\mathrm{A}}^2 + w_{\mathrm{A}}^2}, \tag{2}$$

$$\alpha = \arctan\left(\frac{w_{\mathrm{A}}}{u_{\mathrm{A}}}\right), \tag{3}$$

$$\beta = \arctan\left(\frac{v_{\mathrm{A}}}{\sqrt{u_{\mathrm{A}}^2 + w_{\mathrm{A}}^2}}\right). \tag{4}$$

The airflow angles, i.e., the angle of attack α and the sideslip angle β, are commonly measured by mechanical vanes, while the true airspeed V_{TAS} can be measured by a Pitot-static probe. It is also possible to measure the air triplets by a multi-hole Pitot probe [15].

According to Eqs. (1) to (4), we can formulate a wind estimator as shown in Fig. 2. For the data source of the wind estimator, the kinematic velocity $(u_{\mathrm{K}},\ v_{\mathrm{K}},\ w_{\mathrm{K}})$ and attitude Euler angles $(\phi,\ \theta,\ \psi)$ can be obtained from the navigation system which typically applies the GPS-aided inertial navigation technique with EKF. For offline applications, the ERTSS-based flight path reconstruction [16, 17] can provide these data with lower error covariances utilizing IMU and GPS measurements. The air triplets measurements can be provided by the air data system which consists of Pitot-static probes, vanes, and an air data computer.

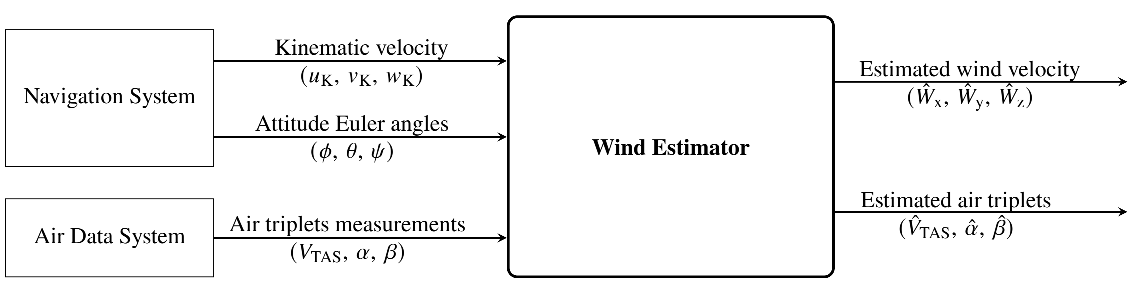

Fig. 2 The wind estimation problem.

III. Adaptive Extended Rauch-Tung-Striebel Smoother

A. Stochastic Modeling of the Wind Velocity

The dynamics of wind velocity is modeled as a random-walk process [8, 9]:

$$
\begin{aligned}
\dot{W}_\mathrm{x} &= w_{W_\mathrm{x}}\,, \\
\dot{W}_\mathrm{y} &= w_{W_\mathrm{y}}\,, \\
\dot{W}_\mathrm{z} &= w_{W_\mathrm{z}}\,.
\end{aligned} \tag{5}
$$

By modeling the wind velocity as a random-walk process, the change rate of the wind velocities with respect to time is stochastically limited by the covariance of noise $\boldsymbol{w}_\mathrm{W}$. In another word, the wind velocity may change more rapidly if the covariance of the noise $\boldsymbol{w}_W$ is larger. Otherwise, if the covariance is small, the wind velocity will change slower and will be closer to a constant value.

B. State Estimation

The system model is formulated in a state-space form with the state vector $\boldsymbol{x}$, the input vector $\boldsymbol{u}$, the output vector $\boldsymbol{y}$, and a process noise vector $\boldsymbol{w}$ as follows:

$$
\boldsymbol{x} = \begin{bmatrix} W_\mathrm{x} & W_\mathrm{y} & W_\mathrm{z} \end{bmatrix}^\top, \tag{6}
$$

$$
\boldsymbol{u} = \begin{bmatrix} u_\mathrm{K} & v_\mathrm{K} & w_\mathrm{K} & \phi & \theta & \psi \end{bmatrix}^\top, \tag{7}
$$

$$
\boldsymbol{y} = \begin{bmatrix} V_\mathrm{TAS} & \alpha & \beta \end{bmatrix}^\top, \tag{8}
$$

$$
\boldsymbol{w} = \begin{bmatrix} w_{W_\mathrm{x}} & w_{W_\mathrm{y}} & w_{W_\mathrm{z}} \end{bmatrix}^\top. \tag{9}
$$

The model of this system can be written in the form of continuous-discrete stochastic equations as

$$
\dot{\boldsymbol{x}}(t) = \boldsymbol{f}(\boldsymbol{x}(t), \boldsymbol{u}(t)) + \boldsymbol{w}(t)\,, \quad \boldsymbol{x}(0) = \boldsymbol{x}_0\,, \tag{10}
$$

$$
\boldsymbol{y}(t) = \boldsymbol{g}(\boldsymbol{x}(t), \boldsymbol{u}(t))\,, \tag{11}
$$

$$
\boldsymbol{z}_k = \boldsymbol{y}_k + \boldsymbol{v}_k\,, \tag{12}
$$

where $\boldsymbol{z}_k$ is the discrete measurement vector. The continuous process noise process $\{\boldsymbol{w}(t)\}$ is assumed to be zero-mean, uncorrelated, white Gaussian with covariance $\mathbb{E}[\boldsymbol{w}(t)\boldsymbol{w}^\top(\tau)] = \boldsymbol{Q}\delta(t-\tau)$, where $\delta(t)$ is the Dirac impulse function. The discrete measurement noise process $\{\boldsymbol{v}_k\}$ is also assumed to be zero-mean, uncorrelated, white Gaussian with covariance $\mathbb{E}[\boldsymbol{v}_j\boldsymbol{v}_k] = \boldsymbol{R}\delta_{jk}$, where δ_{jk} is the Kronecker delta. For the wind estimation problem formulated in this paper, the system dynamic equations Eq. (10) are the wind random-walk model Eq. (5) with $\boldsymbol{f}(\boldsymbol{x}(t), \boldsymbol{u}(t)) = \boldsymbol{0}$. The output equations Eq. (11) stands for the wind triangle equations Eq. (1) together with Eqs. (2) to (4).

The EKF is initialized at the initial time point t_0 with

$$
\hat{\boldsymbol{x}}_{0|0} = \bar{\boldsymbol{x}}_0\,, \tag{13}
$$

$$
\boldsymbol{P}_{0|0} = \bar{\boldsymbol{P}}_0\,, \tag{14}
$$

where $\bar{\boldsymbol{x}}_0$ the a priori estimate of the initial state $\boldsymbol{x}_0$ and $\bar{\boldsymbol{P}}_0 \coloneqq \mathbb{E}\left[(\boldsymbol{x}_0 - \bar{\boldsymbol{x}}_0)(\boldsymbol{x}_0 - \bar{\boldsymbol{x}}_0)^\top\right]$ is the estimation error covariance matrix of $\bar{\boldsymbol{x}}_0$.

The following continuous-discrete EKF equations are sequentially calculated for each discrete time points t_k with $k = 1, \cdots, N$ to obtain filtered state estimates:

$$
\hat{\boldsymbol{x}}_{k|k-1} = \hat{\boldsymbol{x}}_{k-1|k-1} + \int_{t_{k-1}}^{t_k} \boldsymbol{f}(\hat{\boldsymbol{x}}_{k-1|k-1}, \boldsymbol{u}_{k-1})\mathrm{d}t\,, \tag{15}
$$

$$
\boldsymbol{P}_{k|k-1} = \boldsymbol{\Phi}_{k-1}\boldsymbol{P}_{k-1|k-1}\boldsymbol{\Phi}_{k-1}^\top + \boldsymbol{Q}\Delta t_{k-1}\,, \tag{16}
$$

$$
\boldsymbol{K}_k = \boldsymbol{P}_{k|k-1}\boldsymbol{C}_k^\top[\boldsymbol{C}_k\boldsymbol{P}_{k|k-1}\boldsymbol{C}_k^\top + \boldsymbol{R}]^{-1}\,, \tag{17}
$$

$$
\hat{\boldsymbol{x}}_{k|k} = \hat{\boldsymbol{x}}_{k|k-1} + \boldsymbol{K}_k[\boldsymbol{z}_k - \boldsymbol{g}(\hat{\boldsymbol{x}}_{k|k-1}, \boldsymbol{u}_k)]\,, \tag{18}
$$

$$
\boldsymbol{P}_{k|k} = [\boldsymbol{I}_{n_x} - \boldsymbol{K}_k\boldsymbol{C}_k]\boldsymbol{P}_{k|k-1}\,, \tag{19}
$$

where $\hat{\boldsymbol{x}}_{k|k-1} := \mathbb{E}(\boldsymbol{x}_k|z_1, \ldots, z_{k-1})$ is the predicted state estimate, $\boldsymbol{P}_{k|k-1} := \mathbb{E}\left[(\boldsymbol{x}_k - \hat{\boldsymbol{x}}_{k|k-1})(\boldsymbol{x}_k - \hat{\boldsymbol{x}}_{k|k-1})^\top\right]$ is the predicted state error covariance matrix, $\hat{\boldsymbol{x}}_{k|k} := \mathbb{E}(\boldsymbol{x}_k|z_1, \ldots, z_k)$ is the updated state estimate, $\boldsymbol{P}_{k|k} := \mathbb{E}\left[(\boldsymbol{x}_k - \hat{\boldsymbol{x}}_{k|k})(\boldsymbol{x}_k - \hat{\boldsymbol{x}}_{k|k})^\top\right]$ is the updated state error covariance matrix, $\boldsymbol{K}_k$ is the Kalman gain, $\Delta t := t_k - t_{k-1}$ is the sampling period, and I_{n_x} is an n_x-by-n_x identity matrix with n_x being the total number of state components. The integral in Eq. (15) can be solved by the numerical integration schemes, e.g., the classic fourth-order Runge–Kutta method in this paper. The state transition matrix $\boldsymbol{\Phi}_{k-1}$ can be calculated using the linearization matrix $\boldsymbol{A}_{k-1}$ as

$$\boldsymbol{\Phi}_{k-1} = \exp(\boldsymbol{A}_{k-1}\Delta t_{k-1}) \quad \text{with} \quad \boldsymbol{A}_{k-1} = \frac{\partial \boldsymbol{f}(\hat{\boldsymbol{x}}_{k-1|k-1}, \boldsymbol{u}_{k-1})}{\partial \boldsymbol{x}},$$

and the linearization matrix $\boldsymbol{C}_k$ is calculated by

$$\boldsymbol{C}_k = \frac{\partial \boldsymbol{g}(\hat{\boldsymbol{x}}_{k|k-1}, \boldsymbol{u}_k)}{\partial \boldsymbol{x}}.$$

The Rauch-Tung-Striebel smoother [18] is initialized at the final time point t_N using the EKF state estimates and its error covariance for t_N with

$$\hat{\boldsymbol{x}}^{\mathrm{s}}_N = \hat{\boldsymbol{x}}_{N|N}, \tag{20}$$

$$\boldsymbol{P}^{\mathrm{s}}_N = \boldsymbol{P}_{N|N}. \tag{21}$$

The smoother sequentially runs backward in time for the discrete time points t_k with $k = (N-1), \cdots, 0$ to obtain smoothed state estimates as

$$\boldsymbol{K}^{\mathrm{s}}_k = \boldsymbol{P}_{k|k}\boldsymbol{\Phi}_k^\top(\boldsymbol{P}_{k+1|k})^{-1}, \tag{22}$$

$$\hat{\boldsymbol{x}}^{\mathrm{s}}_k = \hat{\boldsymbol{x}}_{k|k} + \boldsymbol{K}^{\mathrm{s}}_k[\hat{\boldsymbol{x}}^{\mathrm{s}}_{k+1} - \hat{\boldsymbol{x}}_{k+1|k}], \tag{23}$$

$$\boldsymbol{P}^{\mathrm{s}}_k = \boldsymbol{P}_{k|k} + \boldsymbol{K}^{\mathrm{s}}_k[\boldsymbol{P}^{\mathrm{s}}_{k+1} - \boldsymbol{P}_{k+1|k}](\boldsymbol{K}^{\mathrm{s}}_k)^\top, \tag{24}$$

where $\hat{\boldsymbol{x}}^{\mathrm{s}}_k := \mathbb{E}(\boldsymbol{x}_k|z_1, \ldots, z_N)$ is the smoothed state estimate and $\boldsymbol{P}^{\mathrm{s}}_k := \mathbb{E}\left[(\boldsymbol{x}_k - \hat{\boldsymbol{x}}^{\mathrm{s}}_k)(\boldsymbol{x}_k - \hat{\boldsymbol{x}}^{\mathrm{s}}_k)^\top\right]$ is the smoothed state error covariance matrix, and $\boldsymbol{K}^{\mathrm{s}}_k$ is the smoother gain.

In addition, the lag-one covariance smoother $\boldsymbol{P}^{\mathrm{s}}_{k,k-1} := \mathbb{E}\left[(\boldsymbol{x}_k - \hat{\boldsymbol{x}}^{\mathrm{s}}_k)(\boldsymbol{x}_{k-1} - \hat{\boldsymbol{x}}^{\mathrm{s}}_{k-1})^\top\right]$ [19] can be calculated by

$$\boldsymbol{P}^{\mathrm{s}}_{N,N-1} = [\boldsymbol{I}_{n_x} - \boldsymbol{K}_N\boldsymbol{C}_N]\boldsymbol{\Phi}_{N-1}\boldsymbol{P}_{N-1|N-1}, \tag{25}$$

$$\boldsymbol{P}^{\mathrm{s}}_{k+1,k} = \boldsymbol{P}_{k+1|k+1}(\boldsymbol{K}^{\mathrm{s}}_k)^\top + \boldsymbol{K}^{\mathrm{s}}_{k+1}[\boldsymbol{P}^{\mathrm{s}}_{k+2,k+1} - \boldsymbol{\Phi}_{k+1}\boldsymbol{P}_{k+1|k+1}](\boldsymbol{K}^{\mathrm{s}}_k)^\top, \quad k = N-2, \cdots, 0. \tag{26}$$

C. Adaptive Noise Covariance Matrices Estimation by the Expectation-Maximization Method

For the ERTSS framework outlined in Section III.B, the tuning parameters that influence the smoothing performance are $(\bar{x}_0, \bar{\boldsymbol{P}}_0, \boldsymbol{Q}, \boldsymbol{R})$. In practice, this is a difficult filter tuning problem, as the process noise covariances of the wind are variant for different flights. Therefore, it would be ideal if these key tuning parameters can be estimated adaptively to improve the overall performance.

An effective proposed solution to the aforementioned problem is the EM method [13, 19]. It is an iterative parameter estimation method based on the maximum likelihood estimation theory that estimates the tuning parameters by using the smoothed residuals from the ERTSS. Hereafter, for simplicity of the notation, we use $\boldsymbol{\Theta}$ to indicate the parameters to be estimated $(\bar{x}_0, \bar{\boldsymbol{P}}_0, \boldsymbol{Q}, \boldsymbol{R})$ in this section. Since the independent multivariate Gaussian distribution assumption made in Section III.B, i.e., the initial states estimate fulfills $\hat{\boldsymbol{x}}_0 \sim \mathcal{N}(\boldsymbol{x}_0, \boldsymbol{P}_0)$, the continuous process noises fulfill $\boldsymbol{w}(t) \sim \mathcal{N}(\boldsymbol{0}, \boldsymbol{Q})$, and the measurement noises fulfill $\boldsymbol{v}_k \sim \mathcal{N}(\boldsymbol{0}, \boldsymbol{R})$, the likelihood function $\mathbb{L}$ for this estimation problem can be written as

$$\begin{aligned}\mathbb{L}(\boldsymbol{\Theta} \,|\, \boldsymbol{x}_{0:N}, z_{1:N}) = {} & \frac{1}{\sqrt{(2\pi)^{n_x}|\boldsymbol{P}_0|}} \exp\left[-\frac{(\hat{\boldsymbol{x}}_0 - \boldsymbol{x}_0)^\top \boldsymbol{P}_0^{-1}(\hat{\boldsymbol{x}}_0 - \boldsymbol{x}_0)}{2}\right] \\ & \times \prod_{k=1}^{N-1} \frac{1}{\sqrt{(2\pi)^{n_w}|\boldsymbol{Q}\Delta t_k|}} \exp\left[-\frac{\boldsymbol{w}_k^\top(\boldsymbol{Q}\Delta t_k)^{-1}\boldsymbol{w}_k}{2}\right] \\ & \times \prod_{k=1}^{N} \frac{1}{\sqrt{(2\pi)^{n_v}|\boldsymbol{R}|}} \exp\left[-\frac{\boldsymbol{v}_k^\top \boldsymbol{R}^{-1}\boldsymbol{v}_k}{2}\right],\end{aligned}$$

where $\boldsymbol{w}_k := \int_{t_k}^{t_{k+1}} \boldsymbol{w}(t)\mathrm{d}t$ is the discretized process noise corresponding to $\boldsymbol{w}(t)$ which fulfills the following Gaussian distribution $\boldsymbol{w}_k \sim \mathcal{N}(\boldsymbol{0}, \boldsymbol{Q}\Delta t_k)$, and n_w and n_v are the number of process and measurement noise components, respectively. The maximum likelihood estimate of the parameters is therefore $\hat{\boldsymbol{\Theta}} = \arg\max_{\boldsymbol{\Theta}} \mathbb{L}(\boldsymbol{\Theta} \,|\, \boldsymbol{x}_{0:N}, z_{1:N})$. The difficulty in solving this equation lies in the fact that the states $\boldsymbol{x}_{0:N}$ that need to be estimated depend on the parameters $\boldsymbol{\Theta}$. To overcome this difficulty, the EM method iteratively updates the parameter values so that the likelihood function value will keep increasing with each iteration. For each iteration, the EM method contains two steps: an expectation step (E-step) and a maximization step (M-step). The E-step runs the ERTSS Eqs. (13) to (26) to find the expectation value of the log-likelihood function $Q(\boldsymbol{\Theta}, \hat{\boldsymbol{\Theta}}^{(j-1)}) := \mathbb{E}[\log \mathbb{L}(\boldsymbol{\Theta} \,|\, \hat{\boldsymbol{x}}_{0:N}(\hat{\boldsymbol{\Theta}}^{(j-1)}), z_{1:N})]$ .The M-step maximizes the log-likelihood function with respect to the parameters $\hat{\boldsymbol{\Theta}}^{(j)} = \arg\max_{\boldsymbol{\Theta}} \mathbb{E}[\log \mathbb{L}(\boldsymbol{\Theta} \,|\, \hat{\boldsymbol{x}}_{0:N}(\hat{\boldsymbol{\Theta}}^{(j-1)}), z_{1:N})]$. Because of the Jensen's inequality and the concavity of the logarithmic function, it can be proven that the EM method guarantees the increase of the likelihood function $\mathbb{L}$ along with successive iterations [13].

The result of the M-step gives the following adaptive estimation equations for the noise covariance $\boldsymbol{Q}$ and $\boldsymbol{R}$ [13]:

$$\hat{\boldsymbol{R}}^{(j)} = \frac{1}{N} \sum_{k=1}^{N} \left[\boldsymbol{r}_k \boldsymbol{r}_k^\top + \boldsymbol{C}_k \boldsymbol{P}_k^{\mathrm{s}} \boldsymbol{C}_k^\top \right] , \tag{27}$$

$$\hat{\boldsymbol{Q}}^{(j)} = \frac{1}{N} \sum_{k=1}^{N} \frac{1}{\Delta t_{k-1}} \left[\boldsymbol{q}_k \boldsymbol{q}_k^\top + \boldsymbol{P}_k^{\mathrm{s}} + \boldsymbol{\Phi}_{k-1} \boldsymbol{P}_{k-1}^{\mathrm{s}} \boldsymbol{\Phi}_{k-1}^\top - \boldsymbol{P}_{k,k-1}^{\mathrm{s}} \boldsymbol{\Phi}_{k-1}^\top - \boldsymbol{\Phi}_{k-1} (\boldsymbol{P}_{k,k-1}^{\mathrm{s}})^\top \right] , \tag{28}$$

where $\boldsymbol{r}_k := z_k - \boldsymbol{h}(\hat{\boldsymbol{x}}_k^{\mathrm{s}}, \boldsymbol{u}_k)$ is the smoothed residual and $\boldsymbol{q}_k := \hat{\boldsymbol{x}}_k^{\mathrm{s}} - \left[\hat{\boldsymbol{x}}_{k-1}^{\mathrm{s}} + \int_{t_{k-1}}^{t_k} \boldsymbol{f}(\hat{\boldsymbol{x}}_{k-1}^{\mathrm{s}}, \boldsymbol{u}_{k-1}) \mathrm{d}t \right]$. The variables on the right-hand side of Eqs. (27) and (28) are calculated in the E-step by the ERTSS Eqs. (13) to (26) with $\hat{\boldsymbol{\Theta}}^{(j-1)}$. The superscripts $(j-1)$ on these variables are omitted for the simplicity of the notations. The initial states and the corresponding estimation error covariance are updated as follows:

$$\hat{\boldsymbol{x}}_{0|0}^{(j)} = (\hat{\boldsymbol{x}}_0^{\mathrm{s}})^{(j-1)} , \tag{29}$$

$$\boldsymbol{P}_{0|0}^{(j)} = (\boldsymbol{P}_0^{\mathrm{s}})^{(j-1)} . \tag{30}$$

The negative log-likelihood function is

$$J_L^{(j)} = \frac{1}{N} \sum_{k=1}^{N} \left(z_k - \boldsymbol{h}(\hat{\boldsymbol{x}}_{k|k-1}) \right)^\top \boldsymbol{S}_k^{-1} \left(z_k - \boldsymbol{h}(\hat{\boldsymbol{x}}_{k|k-1}) \right) + \log(\det(\boldsymbol{S}_k)) , \tag{31}$$

where $\boldsymbol{S}_k = \boldsymbol{C}_k \boldsymbol{P}_{k|k-1} \boldsymbol{C}_k^\top + \hat{\boldsymbol{R}}^{(j-1)}$. The iterations are terminated if the following stopping criterion is reached:

$$\psi^{(j)} = \frac{\left| J_L^{(j)} - J_L^{(j-1)} \right|}{\left| J_L^{(j)} \right|} < \epsilon , \tag{32}$$

where ϵ is a small positive value which is set to be 1×10^{-6} in this paper.

Finally, the adaptive ERTSS algorithm is summarized in a flowchart which is shown in Fig. 3 .

To sum it up, to better solve the wind estimation problem, the adaptive ERTSS algorithm is proposed in this section. The proposed algorithm can adaptively estimate the noise covariance of the wind random-walk, which can be different for each flight, other than chosen based on experience. First, to deal with the stochastic characteristic of wind, the wind velocity is modeled as a random-walk process as in Section III.A. Then, in Section III.B, the random-walk process is embedded into the system model in a state-space form to formulate a state smoothing problem which is solved by the ERTSS Finally, for tuning the noise covariances in the ERTSS to gain better estimation results, the extended EM method is introduced in Section III.C to estimated $\boldsymbol{Q}$ (noise covariance for the wind random-walk) and $\boldsymbol{R}$ (measurement noise covariance for the air triplets).

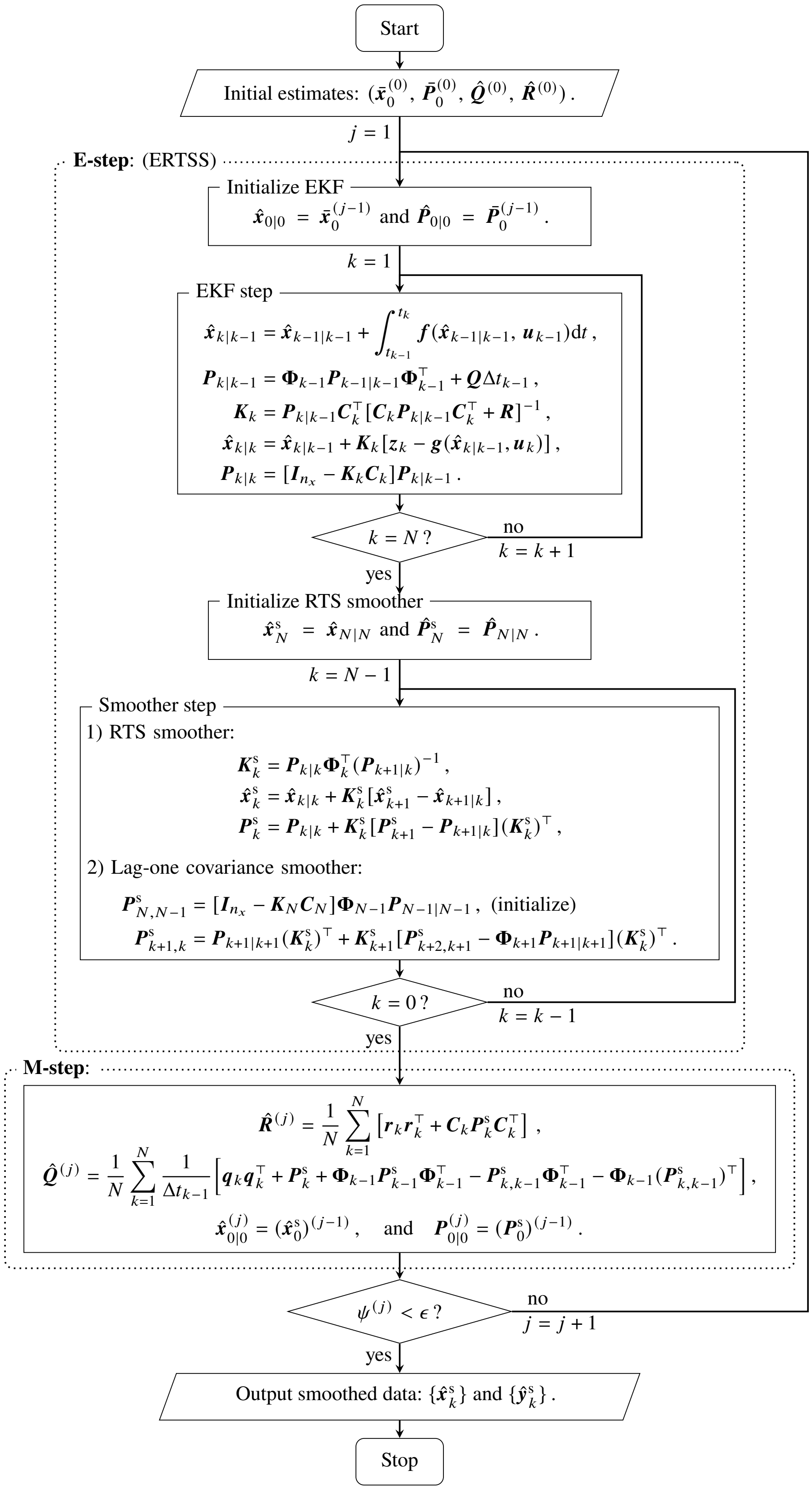

Fig. 3 The flowchart of the adaptive ERTSS algorithm.

IV. Numerical Experiment Results

In this section, the proposed wind estimation algorithm is demonstrated and validated using simulated data. For the test datasets, a kinematic model for rigid-body aircraft is used to generate benchmark flight data. The wind velocity datasets are numerically generated as random-walk processes with different noise levels. After generating the true reference data, zero-mean, uncorrelated, white Gaussian noises are added to the output vector $\boldsymbol{y}$ to formulate the measurement data z for the ERTSS. The measurement noise levels were set to realistic values as shown in Table 1 .

Table 1 The measurement noise standard deviation used in simulated data.

Variables	Sampling Rate [Hz]	Noise Standard Deviation σ	Source
V_{TAS}	100	0.1 m/s	Pitot Tube
α	100	0.2°	Alpha Vane
β	100	0.2°	Beta Vane

The initial state vector is set as $\bar{\boldsymbol{x}}_0^{(0)} = \begin{bmatrix} \hat{W}_x(0) & \hat{W}_y(0) & \hat{W}_z(0) \end{bmatrix}^\top = \mathbf{0}$ m/s , and the initial covariance matrix is set as $\bar{\boldsymbol{P}}_0^{(0)} = 4\boldsymbol{I}_3$ (m/s)^2. The initial estimates for the noise covariance matrices are set to be $\hat{\boldsymbol{Q}}^{(0)} = 1000\boldsymbol{Q}_{\mathrm{true}}$ and $\hat{\boldsymbol{R}}^{(0)} = 1000\boldsymbol{R}_{\mathrm{true}}$. For the implementation of the proposed adaptive ERTSS algorithm, MATLAB® is used with its toolbox MATLAB Coder™ to accelerate the computation by generating MEX functions from the MATLAB code.

The following two scenarios are examined: 1) fully accurate inputs $\boldsymbol{u}$ and 2) inputs $\boldsymbol{u}$ with estimation errors. For the first scenario, we assume that inputs $\boldsymbol{u}$ to be sufficiently accurate to validate the proposed algorithm. This assumption is also made by [7]. Next, in practice, there will still be errors for the kinematic velocity and attitude from the navigation system. Therefore, the second scenario is used to quantify the influence of such estimation errors on wind estimation performance by comparing them with the first scenario. For each of the test scenarios, two different wind-noise levels are examined: a) relatively larger process noises with standard deviation $\sigma(w_W) = 0.1$ (m/s)/$\sqrt{\mathrm{s}}$ and b) relatively smaller wind noise with standard deviation $\sigma(w_W) = 0.01$ (m/s)/$\sqrt{\mathrm{s}}$. As explained in section III.A, larger wind noise indicates that the wind velocity can change faster in a short period, whereas smaller wind noise means that the wind velocity probably changes slower and is more close to a constant.

A. Test Scenario 1: Accurate Inputs

For the first test scenario, we assume data for the adaptive ERTSS inputs $\boldsymbol{u}$, namely the kinematic velocity of the aircraft (u_{K}, v_{K}, w_{K}) and the Euler angles (ϕ, θ, ψ), are fully accurate. In this scenario, two cases with different process noise levels for the wind velocity are presented: a) larger wind noises $\sigma(w_W) = 0.1$ (m/s)/$\sqrt{\mathrm{s}}$ and b) smaller wind noise $\sigma(w_W) = 0.01$ (m/s)/$\sqrt{\mathrm{s}}$, which are marked as Case 1a and Case 1b, respectively. The estimation results of these two cases are presented in Figs. 4 to 7 . The noise covariance parameter estimation results for Cases 1a and 1b are presented in Figs. 4 and 5 , and the state estimation results for smoothed wind velocity and its estimation errors with respect to time t for both cases are presented Figs. 6 and 7 .

As shown in Figs. 4 and 5 , for both cases, the estimated noise covariance matrices $\boldsymbol{Q}$ and $\boldsymbol{R}$ iteratively converge towards their true values with the negative log-likelihood function J_L decreasing. After a certain number of iterations, the stopping criterion terminates the loop when the change of J_L becomes small enough as shown in Figs. 4c and 5c . Comparing Fig. 4 with Fig. 5 , we can observe that Case 1b takes more iterations for the $\boldsymbol{Q}$ values to converge to the close neighborhood of their true values. Our interpretation of this behavior is as follows. Since Case 1b has a lower process noise level compared to Case 1a, the influence of process noises for the smoothed estimates is less significant considering the measurement noise covariance $\boldsymbol{R}$ is the same for both cases. The noise covariance parameter estimation results for both cases are summarized in Table 2 . In this table, the estimated standard deviation (Std) $\hat{\sigma}$ for the process and measurement noises are listed together with their true values σ_{true} between brackets.

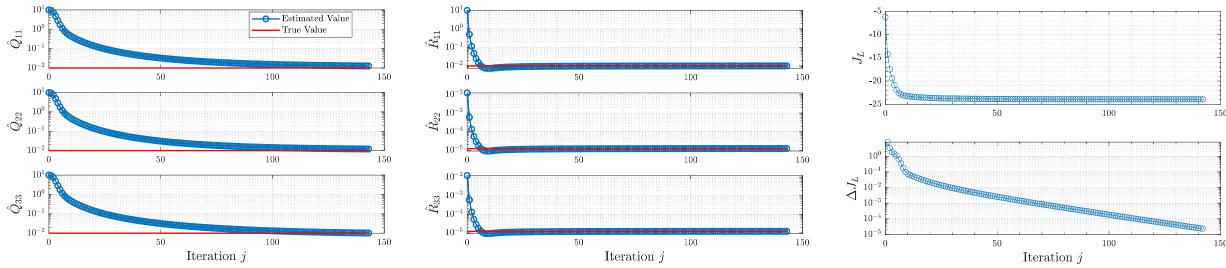

(a) Diagonal elements of $\hat{Q}$. **(b) Diagonal elements of $\hat{R}$.** **(c) Negative log-likelihood function J_L.**

Fig. 4 Case 1a: relatively larger process noise with accurate inputs.

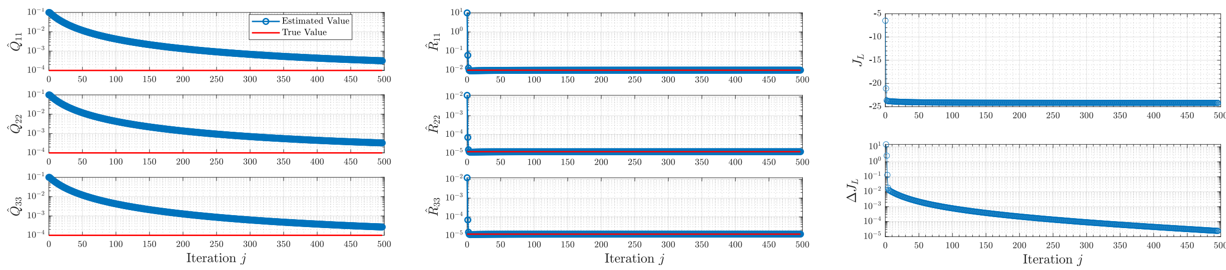

(a) Diagonal elements of $\hat{Q}$. **(b) Diagonal elements of $\hat{R}$.** **(c) Negative log-likelihood function J_L.**

Fig. 5 Case 1b: relatively smaller process noise with accurate inputs.

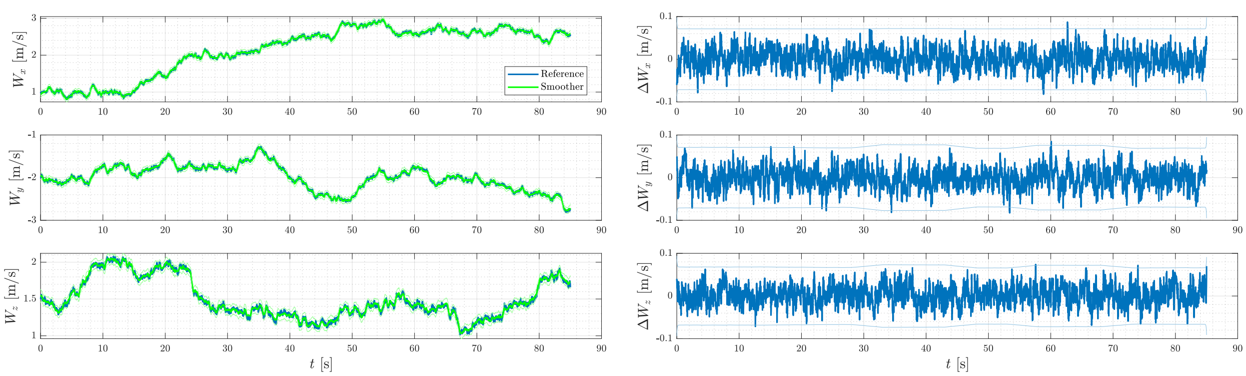

(a) Wind velocity estimation result. **(b) Wind velocity estimation error.**

Fig. 6 Case 1a: relatively larger process noise with accurate inputs.

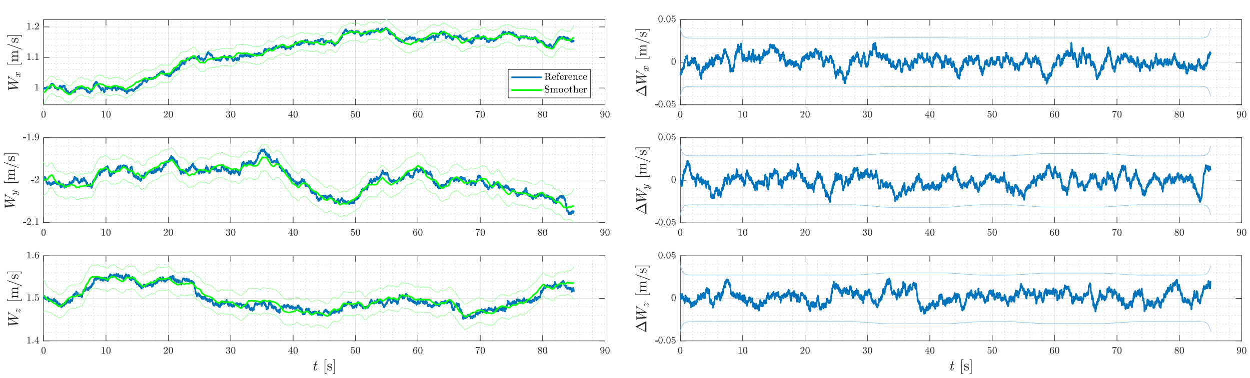

(a) Wind velocity estimation result. **(b) Wind velocity estimation error.**

Fig. 7 Case 1b: relatively smaller process noise with accurate inputs.

Table 2 Estimation results of noise standard deviations for Cases 1a and 1b.

Noise Std	Unit	Case 1a: Larger $\boldsymbol{Q}$		Case 1b: Smaller $\boldsymbol{Q}$	
		$\hat{\sigma}$ (σ_{true})	Ratio $\hat{\sigma}/\sigma_{\text{true}}$	$\hat{\sigma}$ (σ_{true})	Ratio $\hat{\sigma}/\sigma_{\text{true}}$
$\sigma(w_{W_x})$	$(\text{m/s})/\sqrt{\text{s}}$	1.1286×10^{-1} (0.1)	1.1286	1.7793×10^{-2} (0.01)	1.7793
$\sigma(w_{W_y})$	$(\text{m/s})/\sqrt{\text{s}}$	1.0995×10^{-1} (0.1)	1.0995	1.8110×10^{-2} (0.01)	1.8110
$\sigma(w_{W_z})$	$(\text{m/s})/\sqrt{\text{s}}$	1.0089×10^{-1} (0.1)	1.0089	1.6419×10^{-2} (0.01)	1.6419
$\sigma(v_{V_{\text{TAS}}})$	m/s	0.1001 (0.1)	1.0010	0.1003 (0.1)	1.0028
$\sigma(v_\alpha)$	$^\circ$	0.2013 (0.2)	1.0065	0.2004 (0.2)	1.0021
$\sigma(v_\beta)$	$^\circ$	0.2007 (0.2)	1.0035	0.2004 (0.2)	1.0017

After the iterative loop reached the stopping criterion, the ERTSS can use the final estimated noise parameter to estimate the states and outputs optimally. The state estimation results for both Case 1a and Case 1b are shown in Figs. 6 and 7, respectively. For the multiple lines in the same color within the same plot, the solid line in the middle is the adaptive ERTSS estimated (mean) value and the upper and lower thin lines are the estimated 3σ bounds. The wind velocity estimation error is defined as $\Delta \boldsymbol{W} := \hat{\boldsymbol{W}} - \boldsymbol{W}_{\text{true}} = \begin{bmatrix} \Delta W_{\text{x}} & \Delta W_{\text{y}} & \Delta W_{\text{z}} \end{bmatrix}^\top$. From these two figures, we can observe that the ERTSS estimates are close to their true values, as expected. Additionally, for most of the cases, the true values are within the estimated 3σ error bounds.

B. Test Scenario 2: Estimated Inputs

In practice, the kinematic velocity and attitude Euler angles which are estimated by the aircraft's navigation system, as part of the data source of the wind estimator shown in Fig. 2, contain errors that will influence the estimation results. To quantify the influence of such errors, in test scenario 2 the kinematic velocity and attitude Euler angles in the datasets are generated using the estimated values from typical ERTSS-based flight path reconstruction results which contains errors as shown in Fig. 8 . For comparison, the rest of the variables in these test datasets are identical to Cases 1a and 1b. The two corresponding cases in this scenario are referred to as Case 2a and 2b for different wind process noise standard deviations: $\sigma(w_W) = 0.1\ (\text{m/s})/\sqrt{\text{s}}$ (Case 2a) and $\sigma(w_W) = 0.01\ (\text{m/s})/\sqrt{\text{s}}$ (Case 2b).

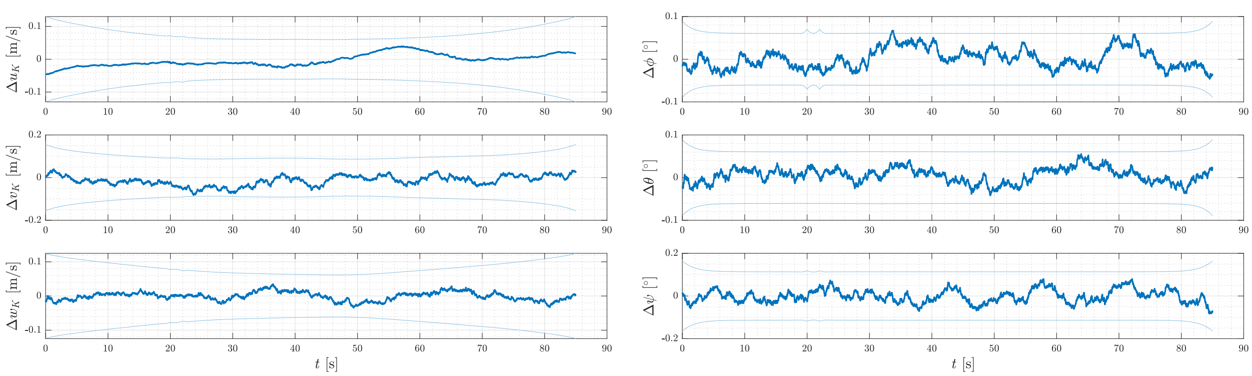

(a) Error of the kinematic velocities. **(b) Error of the Euler angles.**

Fig. 8 Error of the estimated input u for Cases 2a and 2b.

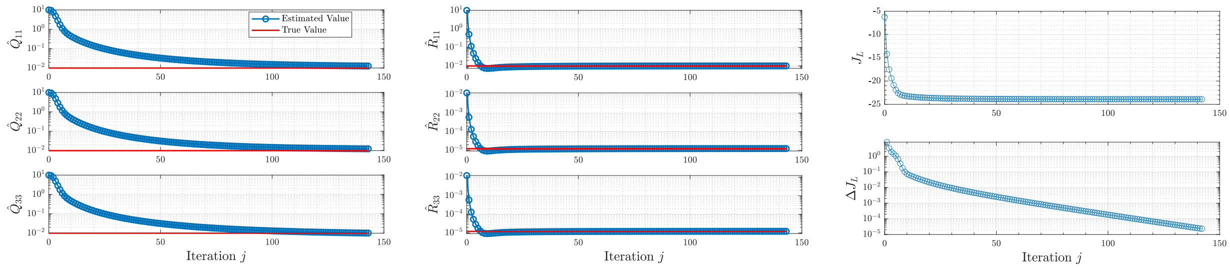

(a) Diagonal elements of $\hat{Q}$. **(b) Diagonal elements of $\hat{R}$.** **(c) Negative log-likelihood function J_L.**

Fig. 9 Case 2a: relatively larger process noise with estimated inputs.

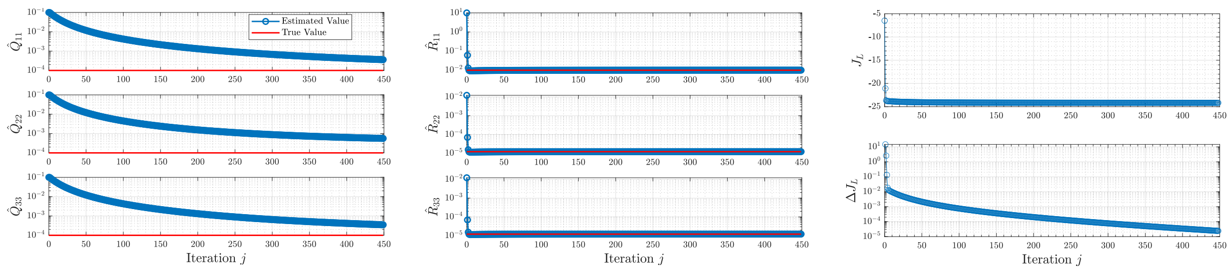

(a) Diagonal elements of $\hat{Q}$ **(b) Diagonal elements of $\hat{R}$** **(c) Negative log-likelihood function J_L.**

Fig. 10 Case 2b: relatively smaller process noise with estimated inputs.

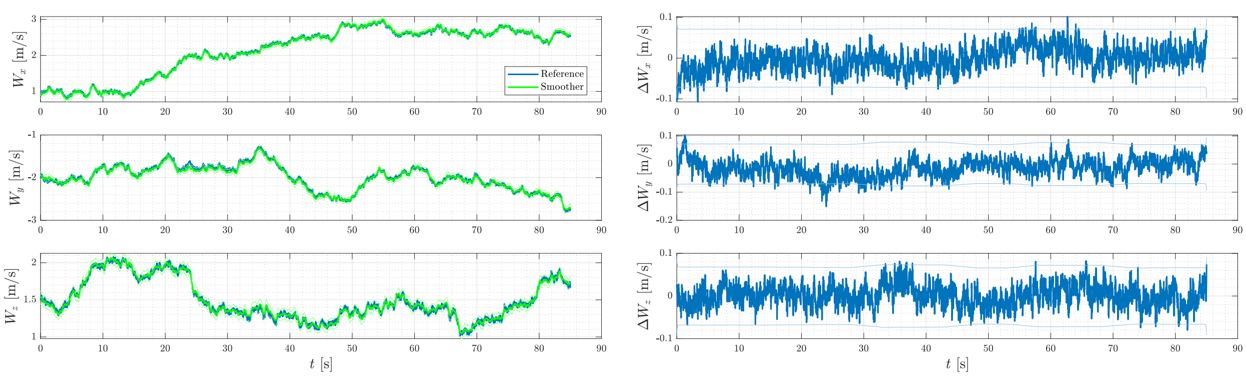

(a) Wind velocity estimation result. **(b) Wind velocity estimation error.**

Fig. 11 Case 2a: relatively larger process noise with estimated inputs.

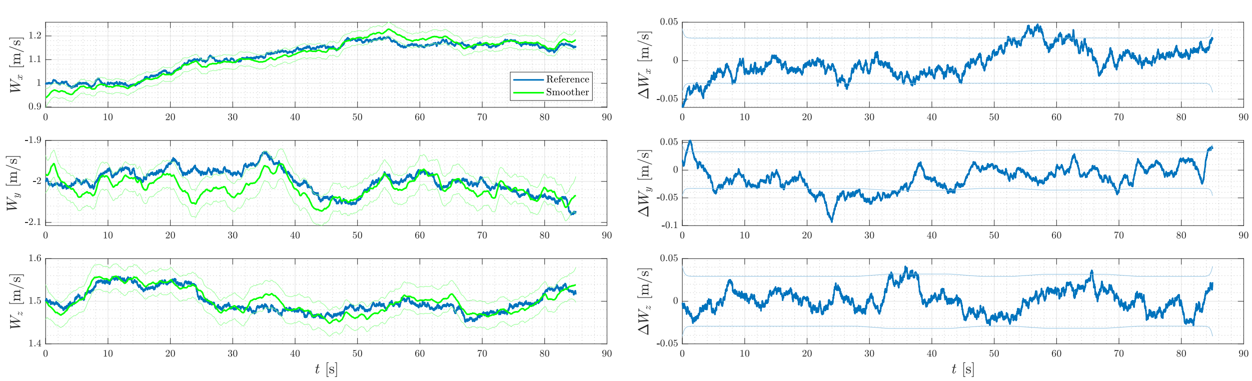

(a) Wind velocity estimation result. **(b) Wind velocity estimation error.**

Fig. 12 Case 2b: relatively smaller process noise with estimated inputs.

The estimation results of these two cases are presented in Figs. 9 to 12 . The noise covariance parameter estimation results for Cases 2a and 2b are presented in Figs. 9 and 10 , and the state estimation results for smoothed wind velocity and its estimation errors for both cases are presented Figs. 11 and 12 . As shown in Figs. 9 and 10 , for both Cases 2a and 2b, with the proposed algorithm the noise covariance matrices converge towards the true value despite the errors in the input data $\boldsymbol{u}$. The estimated values for the noise covariance matrices for Cases 2a and 2b are listed in Table 3 . Comparing results in Tables 2 and 3 , it is clear that the input errors do not have a noticeable influence on the parameter estimation for the two cases with relatively larger process noise covariance $\boldsymbol{Q}$ (comparing Cases 2a with Case 1a). However, for the two cases with relatively smaller process noise covariance $\boldsymbol{Q}$ (comparing Cases 2b with Case 1b), the input errors slightly deteriorate (less than 5%) the estimation of the process noise covariance $\boldsymbol{Q}$.

Table 3 Estimation results of noise standard deviations for Cases 2a and 2b.

Noise Std	Unit	Case 2a: Larger $\boldsymbol{Q}$		Case 2b: Smaller $\boldsymbol{Q}$	
		$\hat{\sigma}$ (σ_{true})	Ratio $\hat{\sigma}/\sigma_{\text{true}}$	$\hat{\sigma}$ (σ_{true})	Ratio $\hat{\sigma}/\sigma_{\text{true}}$
$\sigma(w_{W_x})$	$(\text{m/s})/\sqrt{\text{s}}$	1.1262×10^{-1} (0.1)	1.1262	1.9012×10^{-2} (0.01)	1.9012
$\sigma(w_{W_y})$	$(\text{m/s})/\sqrt{\text{s}}$	1.1122×10^{-1} (0.1)	1.1122	2.3690×10^{-2} (0.01)	2.3690
$\sigma(w_{W_z})$	$(\text{m/s})/\sqrt{\text{s}}$	1.0085×10^{-1} (0.1)	1.0085	1.8730×10^{-2} (0.01)	1.8730
$\sigma(v_{V_{\text{TAS}}})$	m/s	1.0011 (0.1)	1.0011	0.1003 (0.1)	1.0026
$\sigma(v_\alpha)$	°	0.2013 (0.2)	1.0066	0.2004 (0.2)	1.0022
$\sigma(v_\beta)$	°	0.2007 (0.2)	1.0037	0.2006 (0.2)	1.0029

As for the state estimation results, comparing Figs. 6 and 11 for Cases 1a and 2a, we also cannot observe a noticeable change due to the errors in inputs $\boldsymbol{u}$. Nevertheless, from Fig. 12 , it can be seen that there are some biases within the estimated wind velocities for Case 2b, and these errors do not exist for Case 1b as shown Fig. 7 . In addition, if we observe Figs. 8 and 12 together, we can see that the biases in Fig. 12 have the same level of magnitude as the kinematic velocity error shown in Fig. 8a . Therefore, for the cases with smaller wind process noise $\boldsymbol{Q}$, the errors in the input $\boldsymbol{u}$, especially the errors in the estimated kinematic velocity, will to some extent deteriorate the wind estimation accuracy.

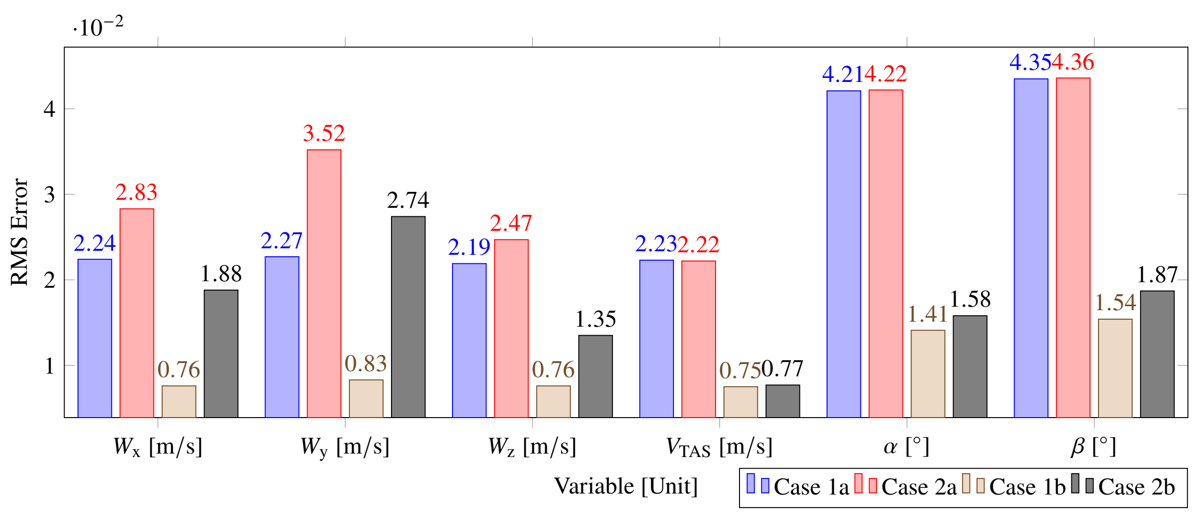

Fig. 13 The RMS error for the smoothed states and outputs.

Finally, to evaluate the estimation accuracy of the proposed method, the root-mean-square (RMS) errors for the smoothed wind velocities and air triplets in each of the four simulations are calculated and summarized in Fig. 13 . First, it can be seen that the estimation errors are influenced by the actual wind noise level. Next, comparing the pair of cases for the same wind noise level (Cases 1a with 2a and Cases 1b with 2b) in Fig. 13 , we can see that the RMS errors for wind velocity estimation are influenced by the errors in the inputs $\boldsymbol{u}$. Whereas, the errors of the estimated $\boldsymbol{u}$ do not distinctly influence the RMS error for the triplets. The magnitude of the influence is similar to the magnitude of the kinematic velocity errors. Last but not least, for V_{TAS}, α and β estimates, the RMS errors for the smoothed values in Fig. 13 are significantly smaller (approximately one order of magnitudes lower) comparing to the measurement noise standard deviation $\sigma(V_{\text{TAS}}) = 0.1$ m/s, $\sigma(\alpha) = 0.2°$, and $\sigma(\beta) = 0.2°$ from Table 1 . Therefore, the accuracy of the air triplets is also improved by applying the proposed adaptive ERTSS algorithm.

V. Conclusion

In this paper, a novel adaptive Extended Rauch-Tung-Striebel Smoother (ERTSS) algorithm for the wind estimation problem using aircraft flight data is proposed. Considering the stochastic nature of the wind, the wind velocity is modeled as a random-walk process with its noise covariance representing the possible changing rate of the wind velocity and embedded into the smoothing framework as state equations. To deal with the fact that the actual noise covariance of the wind random-walk can different in each flight, the extended expectation-maximization method is employed in the wind estimation problem to adaptively estimate the noise covariance matrices $\boldsymbol{Q}$ and $\boldsymbol{R}$ instead of choosing them by experience as previous work. After iteratively estimating the $\boldsymbol{Q}$ and $\boldsymbol{R}$, the adaptive ERTSS can optimally estimate the 3D stochastic wind velocity. Numerical simulation results show the validity of the proposed algorithm. It is demonstrated in the examined cases that the estimated $\boldsymbol{Q}$ and $\boldsymbol{R}$ can converge close to the true value. Besides, the accuracy of the smoothed air triplets: true airspeed, angle of attack, and angle of sideslip data is improved that their RMS errors are approximately one order of magnitudes lower compared to their measurements noise covariances.

References

[1] Langelaan, J. W., Alley, N., and Neidhoefer, J., "Wind Field Estimation for Small Unmanned Aerial Vehicles," *Journal of Guidance, Control, and Dynamics*, Vol. 34, No. 4, 2011, pp. 1016–1030. doi: 10.2514/1.52532.

[2] Witte, B., Singler, R., and Bailey, S., "Development of an Unmanned Aerial Vehicle for the Measurement of Turbulence in the Atmospheric Boundary Layer," *Atmosphere*, Vol. 8, No. 10, 2017, p. 195. doi: 10.3390/atmos8100195.

[3] van Horssen, L., de Visser, C. C., and Pool, D. M., "Aerodynamic Stall and Buffet Modeling for the Cessna Citation II Based on Flight Test Data," *2018 AIAA Modeling and Simulation Technologies Conference*, AIAA, Reston, VA, 2018. doi: 10.2514/6.2018-1167.

[4] van Ingen, J., de Visser, C. C., and Pool, D. M., "Stall Model Identification of a Cessna Citation II from Flight Test Data Using Orthogonal Model Structure Selection," *AIAA Scitech 2021 Forum*, AIAA, Reston, VA, 2021. doi: 10.2514/6.2021-1725.

[5] Myschik, S., and Sachs, G., "Flight Testing an Integrated Wind/Airdata and Navigation System for General Aviation Aircraft," *AIAA Guidance, Navigation and Control Conference and Exhibit*, AIAA, Reston, VA, 2007, p. 6796. doi: 10.2514/6.2007-6796.

[6] Hong, H., Wang, M., Holzapfel, F., and Tang, S., "Fast Real-Time Three-Dimensional Wind Estimation for Fixed-Wing Aircraft," *Aerospace Science and Technology*, Vol. 69, 2017, pp. 674–685. doi: 10.1016/j.ast.2017.07.019.

[7] Cho, Kim, J., Lee, S., and Kee, C., "Wind Estimation and Airspeed Calibration using a UAV with a Single-Antenna GPS Receiver and Pitot Tube," *IEEE Transactions on Aerospace and Electronic Systems*, Vol. 47, No. 1, 2011, pp. 109–117. doi: 10.1109/TAES.2011.5705663.

[8] Rhudy, M. B., Fravolini, M. L., Gu, Y., Napolitano, M. R., Gururajan, S., and Chao, H., "Aircraft Model-Independent Airspeed Estimation without Pitot Tube Measurements," *IEEE Transactions on Aerospace and Electronic Systems*, Vol. 51, No. 3, 2015, pp. 1980–1995. doi: 10.1109/TAES.2015.130631.

[9] Tian, P., Chao, H., Rhudy, M., Gross, J., and Wu, H., "Wind Sensing and Estimation Using Small Fixed-Wing Unmanned Aerial Vehicles: A Survey," *Journal of Aerospace Information Systems*, Vol. 18, No. 3, 2021, pp. 132–143. doi: 10.2514/1.I010885.

[10] Rhudy, M. B., Fravolini, M. L., Porcacchia, M., and Napolitano, M. R., "Comparison of Wind Speed Models within a Pitot-Free Airspeed Estimation Algorithm Using Light Aviation Data," *Aerospace Science and Technology*, Vol. 86, 2019, pp. 21–29. doi: 10.1016/j.ast.2018.12.028.

[11] Myers, K., and Tapley, B., "Adaptive Sequential Estimation with Unknown Noise Statistics," *IEEE Transactions on Automatic Control*, Vol. 21, No. 4, 1976, pp. 520–523. doi: 10.1109/TAC.1976.1101260.

[12] de Mendonça, C. B., Hemerly, E. M., and Góes, L. C. S., "Adaptive Stochastic Filtering for Online Aircraft Flight Path Reconstruction," *Journal of Aircraft*, Vol. 44, No. 5, 2007, pp. 1546–1558. doi: 10.2514/1.27625.

[13] Bavdekar, V. A., Deshpande, A. P., and Patwardhan, S. C., "Identification of Process and Measurement Noise Covariance for State and Parameter Estimation Using Extended Kalman Filter," *Journal of Process Control*, Vol. 21, No. 4, 2011, pp. 585–601. doi: 10.1016/j.jprocont.2011.01.001.

[14] Ananthasayanam, M. R., Mohan, M. S., Naik, N., and Gemson, R. M. O., "A Heuristic Reference Recursive Recipe for Adaptively Tuning the Kalman Filter Statistics Part-1: Formulation and Simulation Studies," *Sādhanā*, Vol. 41, No. 12, 2016, pp. 1473–1490. doi: 10.1007/s12046-016-0562-z.

[15] Sankaralingam, L., and Ramprasadh, C., "A Comprehensive Survey on the Methods of Angle of Attack Measurement and Estimation in UAVs," *Chinese Journal of Aeronautics*, Vol. 33, No. 3, 2020, pp. 749–770. doi: 10.1016/j.cja.2019.11.003.

[16] Mulder, J. A., Chu, Q. P., Sridhar, J. K., Breeman, J. H., and Laban, M., "Non-linear Aircraft Flight Path Reconstruction Review and New Advances," *Progress in Aerospace Sciences*, Vol. 35, No. 7, 1999, pp. 673–726. doi: 10.1016/S0376-0421(99)00005-6.

[17] Jategaonkar, R. V., *Flight Vehicle System Identification: A Time-Domain Methodology, Second Edition*, American Institute of Aeronautics and Astronautics, Reston, VA, 2015. doi: 10.2514/4.102790.

[18] Rauch, H. E., Tung, F., and Striebel, C. T., "Maximum Likelihood Estimates of Linear Dynamic Systems," *AIAA Journal*, Vol. 3, No. 8, 1965, pp. 1445–1450. doi: 10.2514/3.3166.

[19] Shumway, R. H., and Stoffer, D. S., *Time Series Analysis and Its Applications: With R Examples*, 4^{th} ed., Springer International Publishing, Cham, Switzerland, 2017. doi: 10.1007/978-3-319-52452-8.